

# Effects of Annealing Temperature on the Electrochemical Hydrogen Storage Behaviors of La-Mg-Ni-Based $A_2B_7$ -Type Electrode Alloys

YANGHUAN ZHANG, ZEMING YUAN, TINGTING ZHAI, TAI YANG, WENGANG BU, and SHIHAI GUO

In an attempt to improve the cyclic stability of La-Mg-Ni-based  $A_2B_7$ -type electrode alloys,  $La_{0.8}Mg_{0.2}Ni_{3.3}Co_{0.2}Si_x$  ( $x = 0-0.2$ ) electrode alloys were fabricated by casting and annealing, and the effects of annealing temperature on the structures and electrochemical hydrogen storage performances of the alloys were systematically investigated. The results indicate that the as-cast and annealed alloys exhibit multiple structures that contain two major phases,  $(La,Mg)_2Ni_7$  with a  $Ce_2Ni_7$ -type hexagonal structure and  $LaNi_5$  with a  $CaCu_5$ -type hexagonal structure; and one residual phase,  $LaNi_3$ . Both the lattice constants and cell volumes of the two major phases increase with the increasing annealing temperature. Instead of altering the phase composition, the annealing treatment causes the abundances of these two major phases to vary. Based on electrochemical measurements, the cycle stabilities of the alloys are found to be considerably improved by annealing, and the alloy's discharge capacity yields a maximum value with the increasing annealing temperature due to the variation in phase abundance and the homogenization of the composition, respectively. The influence of the annealing treatment on the electrochemical kinetics of the alloys is associated with the alloy's composition; the electrochemical kinetics of the Si-free alloy become slower with the increasing annealing temperature, whereas those of the Si-added alloys first mount up and then go down under the same conditions.

DOI: 10.1007/s11661-015-2788-5

© The Minerals, Metals & Materials Society and ASM International 2015

## I. INTRODUCTION

DUE to their major advantages including high-energy density, excellent power density, and long cycle life, Ni/MH batteries are considered to be promising candidates as battery power sources for electric vehicles (EVs).<sup>[1]</sup> A series of metal hydride electrode materials including the rare-earth-based  $AB_5$ -type alloys,<sup>[2]</sup>  $AB_2$ -type Laves phase alloys,<sup>[3]</sup> V-based solid solution alloys,<sup>[4]</sup> and Mg-based alloys<sup>[5]</sup> are the potential electrode materials for on-board vehicle applications. In particular, the rare earth-based  $AB_5$ -type alloys have been industrialized on large scales in China and Japan. However, among the above-mentioned electrode materials, there is no perfect choice that meets all the needs for transportation applications due to their limiting properties such as the low discharge capacity of the  $AB_5$ -type alloy,<sup>[6]</sup> the poor activation capabilities of the

$AB_2$ -type Laves phase<sup>[7]</sup> and V-based solid solution alloys,<sup>[8]</sup> and the poor cycle stability of the Mg-based electrode alloy.<sup>[9,10]</sup> Hence, the development of new electrode materials with superior performances has become increasingly urgent. Currently, based on the reports of Kadir *et al.*<sup>[11]</sup> and Kohno *et al.*,<sup>[12]</sup> La-Mg-Ni-system  $A_2B_7$ -type alloys are thought to be the most promising candidates for the negative electrode materials of Ni-MH rechargeable batteries due to their high discharge capacities (380 to 410 mAh/g) and low production costs. Encouraged by their high hydrogen-storage capacity and the financial support through programs such as the National High Technology Research and Development Program of China ("863" Program for short), intensive research has been undertaken to promote the industrialization of La-Mg-Ni-system  $A_2B_7$ -type alloys. Although considerable progress has been achieved, as summarized by Liu *et al.*,<sup>[13,14]</sup> the development of La-Mg-Ni-system  $A_2B_7$ -type alloys has been hindered by their poor cycle stability, and a suitable alloy of this type has not yet been identified as the negative electrode for Ni-MH batteries. Researchers still face a serious challenge in enhancing the cycle stability of the alloy without reducing its discharge capacity.

It has come to light that the capacity deterioration in La-Mg-Ni system alloy electrodes is mainly attributed to the pulverization of the alloy particles and the oxidation/corrosion of Mg and La.<sup>[13]</sup> Elemental substitution

YANGHUAN ZHANG, Professor, is with the Key Laboratory of Integrated Exploitation of Baiyun Obo Multi-Metal Resources, Inner Mongolia University of Science and Technology, 7 Aerding Avenue, Baotou 014010, P.R. China, and also with the Department of Functional Material Research, Central Iron and Steel Research Institute, 76 Xueyuannan Road, Beijing 100081, P.R. China. Contact e-mail: zhangyh59@sina.com ZEMING YUAN, TINGTING ZHAI, TAI YANG, and WENGANG BU, Doctoral Students, and SHIHAI GUO, Researcher, are with the Department of Functional Material Research, Central Iron and Steel Research Institute.

Manuscript submitted February 19, 2014.

Article published online February 11, 2015

or addition is an effective method for improving the overall properties of hydrogen storage alloys. For example, the partial replacements of Ni with Co, Fe, Mn, Al, and Cu<sup>[15,16]</sup>; La with Ce, Pr, and Nd<sup>[17–19]</sup>; and Mg with Ca<sup>[20]</sup> have been systematically studied. The addition of Si can ameliorate the anti-oxidation and anti-corrosion abilities of the alloy and improve the cycle stability due to the formation of a dense silicon oxide film on the surface of the alloy electrode.<sup>[21]</sup> Moreover, the fabrication technology is also extremely vital for improving alloy performance. Huang *et al.*<sup>[22]</sup> reported that annealing changes the phase composition, increases the capacity, and improves the plateau performance of La-Mg-Ni-based A<sub>2</sub>B<sub>7</sub>-type electrode alloys. Hence, we expect that the combination of the addition of an optimized amount of Si and a proper annealing temperature may yield an alloy with superior electrochemical performance. To validate this, the effects of Si content and annealing temperature on the structures and electrochemical hydrogen storage performances of La<sub>0.8</sub>Mg<sub>0.2</sub>Ni<sub>3.3</sub>Co<sub>0.2</sub>Si<sub>x</sub> ( $x = 0$  to 0.2) electrode alloys have been systematically investigated.

## II. EXPERIMENTAL

### A. Alloy Preparation

The La, Ni, Co, Mg, and Si as raw materials had purities of at least 99.8 pct, and the chemical compositions of the electrode alloys were La<sub>0.8</sub>Mg<sub>0.2</sub>Ni<sub>3.3</sub>Co<sub>0.2</sub>Si<sub>x</sub> ( $x = 0$  to 0.2). For convenience, the alloys were denoted in terms of Si content as Si<sub>0</sub>, Si<sub>0.05</sub>, Si<sub>0.1</sub>, Si<sub>0.15</sub>, and Si<sub>0.2</sub>. The alloy ingots were prepared using a vacuum induction furnace in a helium atmosphere at a pressure of 0.04 MPa to prevent Mg from volatilizing during the melting. The alloys were annealed at temperatures of 1173 K, 1223 K, 1273 K, and 1323 K (900 °C, 950 °C, 1000 °C, 1050 °C) for 8 hours in vacuum.

### B. Microstructural Characterization

The phases and compositions of the as-cast and annealed alloys were characterized by X-ray diffraction (XRD: Rigaku D/max/2400) using Cu-K<sub>α1</sub> radiation ( $\lambda = 0.15418$  Å) filtered by graphite at 160 mA, 40 kV, and 10°/min. The morphologies and compositions of the as-cast and annealed alloys were examined by scanning electron microscope (SEM: FEI QUANTA 400) and energy-dispersive X-ray spectroscopy (EDS: EDAX Apollo 40 silicon drift detector).

### C. Electrochemical Measurements

#### 1. Samples for testing

Round electrode pellets with diameter of 15 mm were prepared by cold pressing the mixture of the alloy powder and carbonyl nickel powder with the weight ratio of 1:4 under a pressure of 35 MPa. After drying for 4 hours, the electrode pellets were immersed in a 6 M KOH solution for 24 hours in order to fully wet the electrodes before electrochemical measurements.

The cycle stability, activation capability, and discharge capacity were performed in a battery test system (LAND-CT2001A) at 303 K (30 °C) by using a tri-electrode open cell consisting of a working electrode (the metal hydride electrode), a sintered Ni(OH)<sub>2</sub>/NiOOH counter electrode, and an Hg/HgO reference electrode, which were immersed in the electrolyte of 6 M KOH, and the potential difference between the negative and reference electrode is defined as the discharge voltage. In every charge–discharge cycle, the alloy electrode was first charged with a constant current density. After resting for 15 min, it was discharged with the same current density to the cut-off voltage of  $-0.500$  V.

The electrochemical impedance spectra (EIS) and the Tafel polarization curves of the alloys were measured using an electrochemical workstation (PARSTAT 2273). The fresh electrodes were fully charged and then allowed to rest for 2 h to reach open-circuit potential stabilization. For the collection of EIS, the frequency ranged from 10 kHz to 5 mHz at a 50 pct depth of discharge (DOD), the amplitude of signal potentiostatic or galvanostatic measurements was 5 mV, and the number of points per decade of frequencies was 60. For the Tafel polarization curves, the potential ranged from  $-1.2$  to  $+1.0$  V (*vs* Hg/HgO) with a scan rate of 5 mV/s. For the potentiostatic discharge, the test electrodes in the fully charged state were discharged at 500 mV potential steps for 5000 seconds on an electrochemical workstation (PARSTAT 2273) using electrochemistry corrosion software (CorrWare).

## III. RESULTS AND DISCUSSION

### A. Structural Characteristics

As shown in Figure 1, the XRD profiles of the as-cast and annealed La<sub>0.8</sub>Mg<sub>0.2</sub>Ni<sub>3.3</sub>Co<sub>0.2</sub>Si<sub>x</sub> ( $x = 0$  to 0.2) alloys indicate that all the alloys possess multiphase structures with two major phases, (La,Mg)<sub>2</sub>Ni<sub>7</sub> and LaNi<sub>5</sub>, as well as a residual phase LaNi<sub>3</sub>. The annealing treatment hardly changes the component phases, but it significantly changes the abundances of the different phases. Table I lists the lattice parameters along with the abundances of the (La,Mg)<sub>2</sub>Ni<sub>7</sub> and LaNi<sub>5</sub> phases in the alloys, which were calculated from the XRD data using Jade 6.0 software. The annealing treatment clearly increases the lattice constants and cell volumes of the two major phases. Furthermore, annealing also induces a notable change in the abundances of the different alloy phases: the abundance of (La,Mg)<sub>2</sub>Ni<sub>7</sub> first increases and then decreases with the increasing annealing temperature, while the opposite trend (an initial decrease followed by an increase) is observed for the LaNi<sub>5</sub> phase.

The SEM images of the as-cast and annealed Si<sub>0</sub> and Si<sub>0.15</sub> alloys are presented in Figure 2. Apparently, the dendritic morphologies of the as-cast Si<sub>0</sub> and Si<sub>0.15</sub> alloys exhibit obvious changes after annealing at different temperatures. In particular, when the annealing temperature increases to 1323 K (1050 °C), the grains of the alloys become very coarse. According to XRD, SEM, and EDS

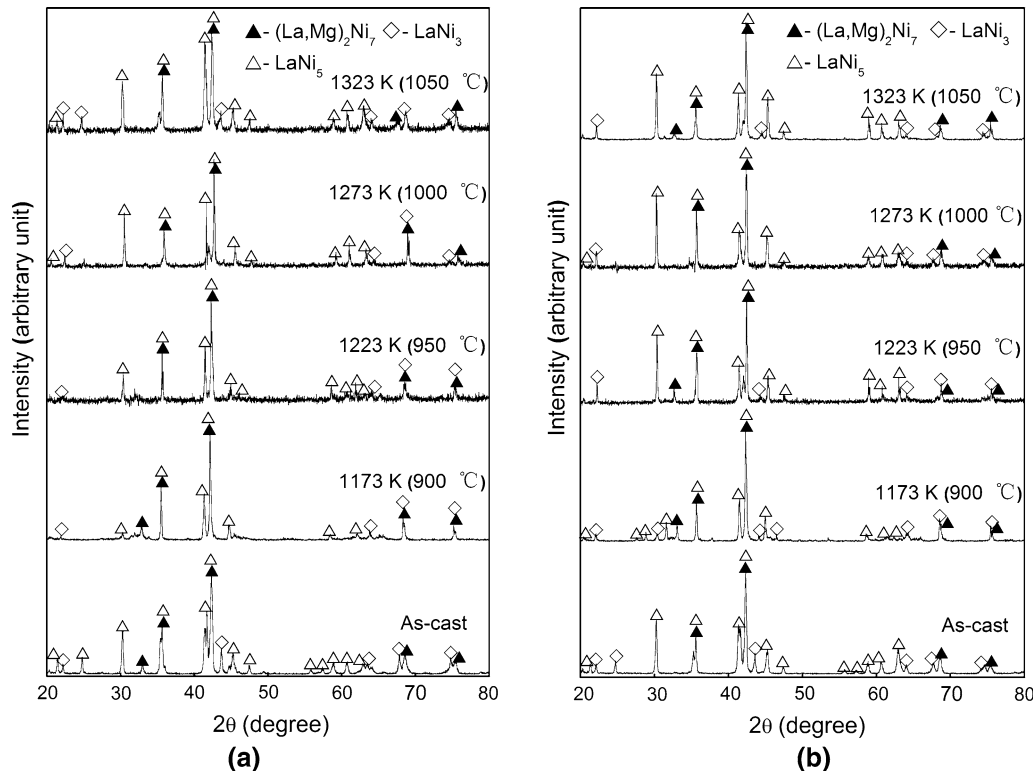


Fig. 1—XRD profiles of the as-cast and annealed  $\text{La}_{0.8}\text{Mg}_{0.2}\text{Ni}_{3.3}\text{Co}_{0.2}\text{Si}_x$  ( $x = 0-0.2$ ) alloys: (a)  $\text{Si}_0$  and (b)  $\text{Si}_{0.15}$ .

Table I. Lattice Parameters, Abundances of Major Phases  $(\text{La}, \text{Mg})_2\text{Ni}_7$  and  $\text{LaNi}_5$

Alloys	Annealing Temperature	Major Phases	Lattice Constants (nm)		Cell Volumes ( $\text{nm}^3$ )	Phase Abundance (Wt Pct)
			<i>a</i>	<i>c</i>		
$\text{Si}_0$	As-cast	$(\text{La}, \text{Mg})_2\text{Ni}_7$	0.5062	2.4568	0.5452	73.2
		$\text{LaNi}_5$	0.5037	0.4002	0.0879	22.6
	1173 K (900 °C)	$(\text{La}, \text{Mg})_2\text{Ni}_7$	0.5065	2.4569	0.5458	76.2
		$\text{LaNi}_5$	0.5040	0.4006	0.0881	19.6
	1223 K (950 °C)	$(\text{La}, \text{Mg})_2\text{Ni}_7$	0.5066	2.4571	0.5461	74.3
		$\text{LaNi}_5$	0.5042	0.4007	0.0882	20.2
1273 K (1000 °C)	$(\text{La}, \text{Mg})_2\text{Ni}_7$	0.5067	2.4572	0.5463	70.6	
	$\text{LaNi}_5$	0.5043	0.4009	0.0883	25.8	
1323 K (1050 °C)	$(\text{La}, \text{Mg})_2\text{Ni}_7$	0.5068	2.4572	0.5466	68.2	
	$\text{LaNi}_5$	0.5044	0.4011	0.0884	28.3	
$\text{Si}_{0.15}$	As-cast	$(\text{La}, \text{Mg})_2\text{Ni}_7$	0.5064	2.4571	0.5457	61.4
		$\text{LaNi}_5$	0.5053	0.4019	0.0889	33.3
	1173 K (900 °C)	$(\text{La}, \text{Mg})_2\text{Ni}_7$	0.5068	2.4573	0.5466	64.4
		$\text{LaNi}_5$	0.5055	0.4023	0.0890	30.3
	950 K (950 °C)	$(\text{La}, \text{Mg})_2\text{Ni}_7$	0.5068	2.4573	0.5466	63.2
		$\text{LaNi}_5$	0.5056	0.4024	0.0891	32.3
1273 K (1000 °C)	$(\text{La}, \text{Mg})_2\text{Ni}_7$	0.5069	2.4574	0.5468	59.6	
	$\text{LaNi}_5$	0.5057	0.4025	0.0891	35.1	
1323 K (1050 °C)	$(\text{La}, \text{Mg})_2\text{Ni}_7$	0.5070	2.4575	0.5471	57.6	
	$\text{LaNi}_5$	0.5059	0.4026	0.0892	38.1	

results, all the experimental alloys have multiphase structures containing  $(\text{La}, \text{Mg})_2\text{Ni}_7$  (denoted as A),  $\text{LaNi}_5$  (denoted as B), and  $\text{LaNi}_3$  (denoted as C) phases. In addition, the intensity of the Si peak in Figure 2(h) is greater

than that in Figure 2(g), indicating that the Si concentration in the  $\text{LaNi}_5$  phase is clearly higher than that in the  $(\text{La}, \text{Mg})_2\text{Ni}_7$  phase. This implies that Si prefers to form a solid solution with the  $\text{LaNi}_5$  phase.

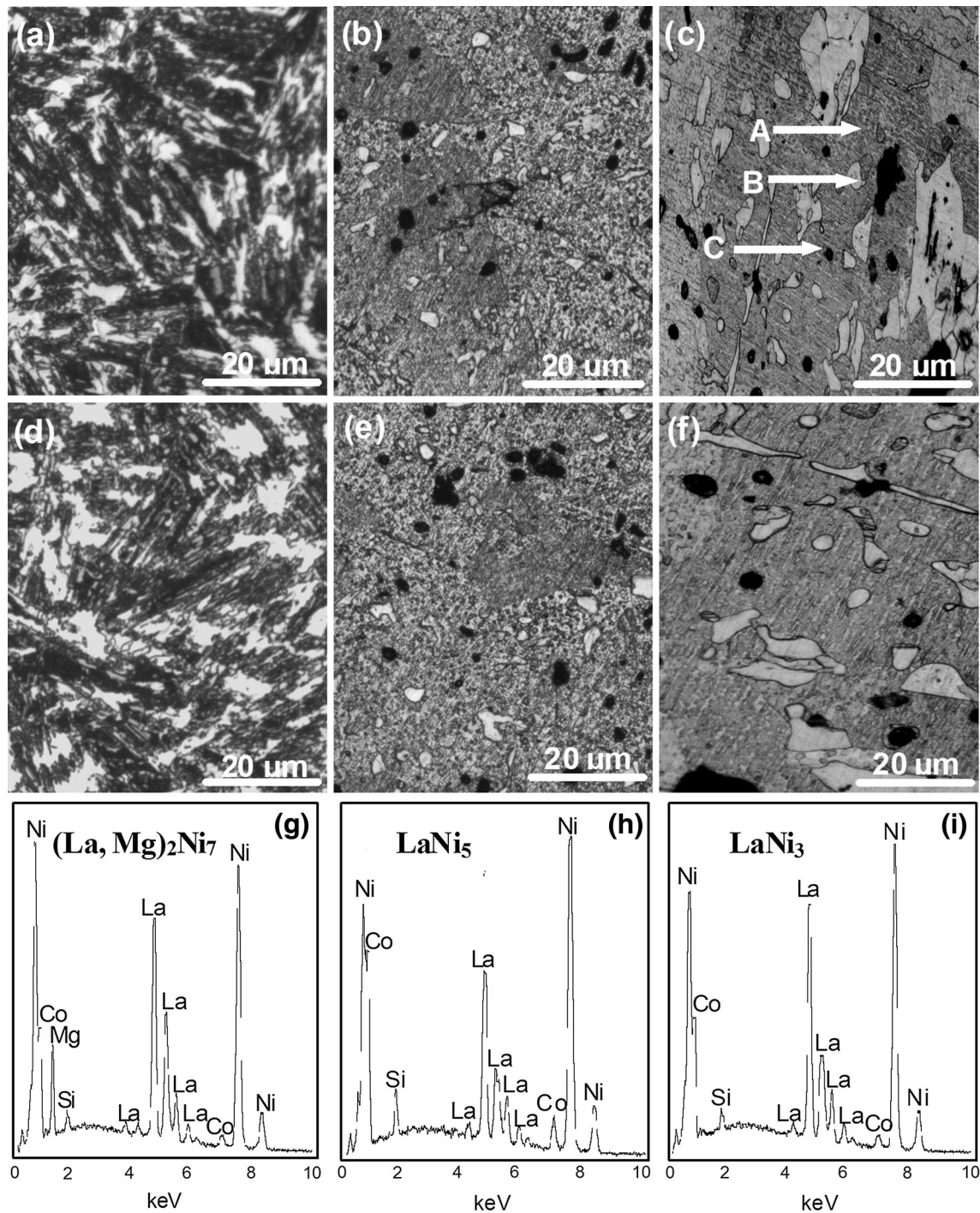


Fig. 2—SEM images of the as-cast and annealed Si<sub>0</sub> and Si<sub>0.15</sub> alloys along with typical EDS patterns: (a) as-cast Si<sub>0</sub>; (b) as-annealed Si<sub>0</sub> [1173 K (900 °C)]; (c) as-annealed Si<sub>0</sub> [1323 K (1050 °C)]; (d) as-cast Si<sub>0.15</sub>; (e) as-annealed Si<sub>0.15</sub> [1173 K (900 °C)]; (f) as-annealed Si<sub>0.15</sub> [1323 K (1050 °C)]; (g, h, i) EDS spectra of positions A, B, and C indicated by arrows in Fig. 2(c), respectively.

## B. Electrochemical Hydrogen Storage Performance

### 1. Cycle stability

The cycle life of the electrode alloy is characterized by the cycle number when the discharge capacity is reduced to 60 pct of the maximum capacity and is a decisive factor for the application of the electrode in Ni-MH batteries. Evidently, the greater the number of charging–

discharging cycle is, the better the cycle life will be. The evolutions of the discharge capacities of the as-cast and annealed La<sub>0.8</sub>Mg<sub>0.2</sub>Ni<sub>3.3</sub>Co<sub>0.2</sub>Si<sub>x</sub> ( $x = 0$  to 0.2) alloys with cycle number are demonstrated in Figure 3, wherein the degradation process of the discharge capacity of the alloys can be seen clearly. The slopes of the curves qualitatively reflect the degradation rate of the discharge

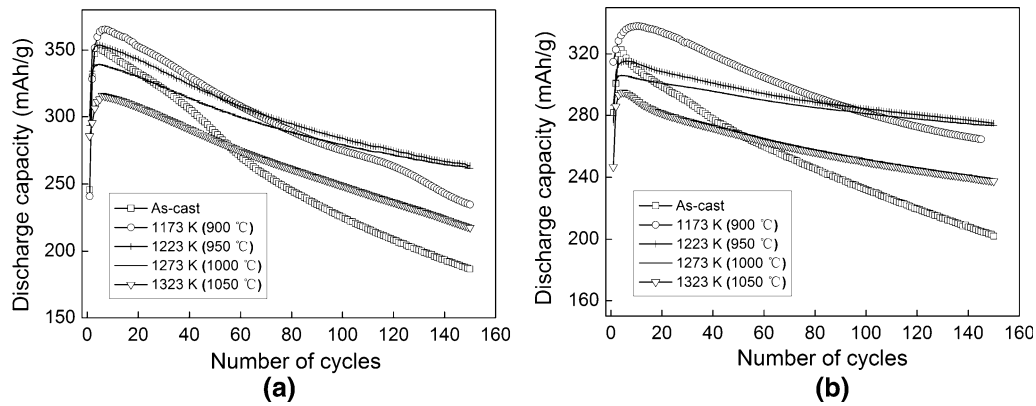


Fig. 3—Discharge capacities of the  $\text{La}_{0.8}\text{Mg}_{0.2}\text{Ni}_{3.3}\text{Co}_{0.2}\text{Si}_x$  ( $x = 0$  to  $0.2$ ) alloys as functions of cycle number: (a)  $\text{Si}_0$  alloy and (b)  $\text{Si}_{0.15}$  alloy.

**Table II. The Slope of Discharge Capacity Curves for Degradation Process**

	As-cast	1173 K (900 °C)	950 K (950 °C)	1273 K (1000 °C)	1323 K (1050 °C)
$\text{Si}_0$ alloys	-1.1866	-0.89633	-0.63577	-0.54716	-0.69121
$\text{Si}_{0.15}$ alloys	-0.76902	-0.57805	-0.26805	-0.22495	-0.36063

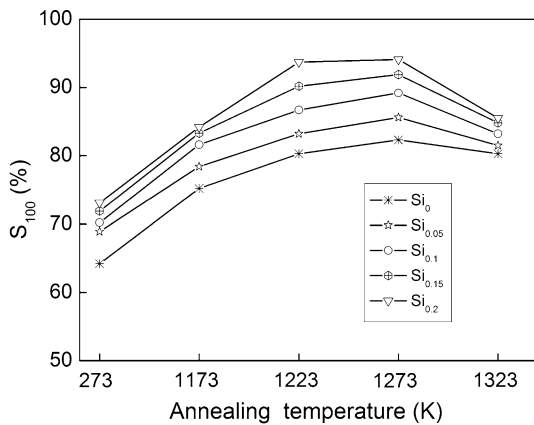


Fig. 4— $S_{100}$  values of the  $\text{La}_{0.8}\text{Mg}_{0.2}\text{Ni}_{3.3}\text{Co}_{0.2}\text{Si}_x$  ( $x = 0$  to  $0.2$ ) alloys as functions of annealing temperature.

capacity during the charge–discharge cycles (as listed in Table II); a smaller curve slope is associated with a better cycle life of the alloy. We note that the slope of the curve clearly decreases with the increasing annealing temperature up to 1273 K (1000 °C); however, when the temperature is further increased to 1323 K (1050 °C), an undesired augment appears. Furthermore, regardless of annealing temperature, the slope of the curve of the as-annealed alloy is always less than that of the as-cast one, and the slope of  $\text{Si}_{0.15}$  alloys is also less than that of  $\text{Si}_0$  alloys, indicating that the annealing treatment and the addition of Si have positive effects on the cycle life of the alloy electrode.

In order to establish a relationship between alloy cycle stability and annealing temperature, the capacity retaining rate ( $S_{100}$ ), defined as  $S_{100} = C_{100}/C_{\text{max}} \times 100$  pct, where  $C_{\text{max}}$  is the maximum discharge capacity, and  $C_{100}$  is the discharge capacity at the 100th cycle with a current density of 300 mA/g, is introduced to accurately

evaluate the cycle stability of the alloy. The  $S_{100}$  values of the  $\text{La}_{0.8}\text{Mg}_{0.2}\text{Ni}_{3.3}\text{Co}_{0.2}\text{Si}_x$  ( $x = 0$  to  $0.2$ ) alloys at different annealing temperatures are shown in Figure 4. The  $S_{100}$  values of the alloys clearly augment with the annealing temperature rising to 1273 K (1000 °C); however, when the temperature reaches 1323 K (1050 °C), an undesired decline in  $S_{100}$  is observed. In spite of this, the  $S_{100}$  values of all the as-annealed alloys are always higher than those of the as-cast ones, suggesting that the annealing treatment is beneficial to alloy cycle stability. In addition, we find whatever the annealing temperature is, the  $S_{100}$  value of the alloy always increases with the increasing Si content, indicating that the addition of Si positively affects alloy cycle stability.

Some explanations as regards why cycle stability is improved by annealing are provided as follows. Normally, the failure of an electrode is characterized by the decay of discharge capacity and drop in discharge voltage.<sup>[23]</sup> The degradation of the discharge capacity in  $\text{A}_2\text{B}_7$ -type alloy electrodes primarily originates from the forming and continuous thickening of  $\text{Mg}(\text{OH})_2$  and  $\text{La}(\text{OH})_2$  surface layers, which hinder the hydrogen atoms from diffusing in or out, in alkaline solutions.<sup>[24]</sup> In addition, hydrogen storage alloys suffer from volume changes during the charging–discharging process. This inevitably aggravates the cracking and pulverization of the alloy, which consequently facilitates the oxidation of the alloy surface. The positive effect of annealing on cycle stability is attributed to the enlarged cell volume and the more homogeneous composition distribution, which retard alloy pulverization and improve the cycle stability of the alloy electrode. Annealing at a higher temperatures such as 1323 K (1050 °C) will inevitably cause grain coarsening, which is responsible for the decreased  $S_{100}$  value of the alloy because coarse grains are harmful to cycle stability. As reported by Sakai *et al.*,<sup>[25]</sup> the formation of passivation layers on the grain

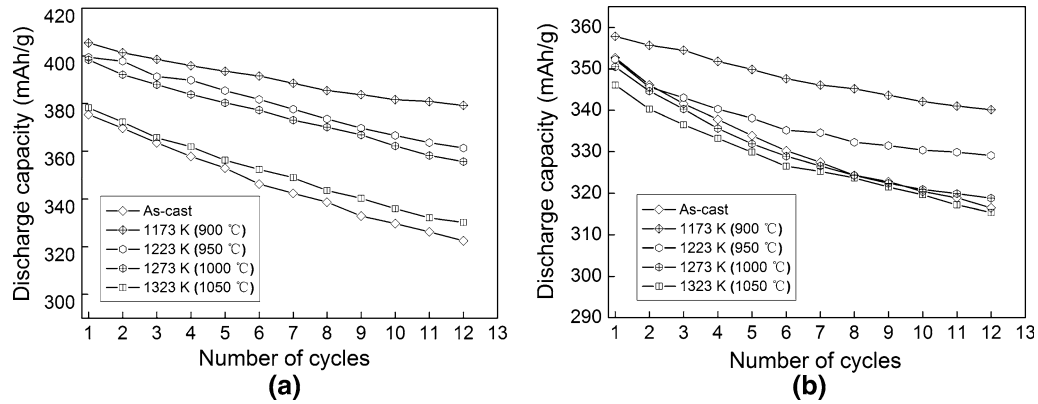


Fig. 5—Activation capabilities of the  $\text{La}_{0.8}\text{Mg}_{0.2}\text{Ni}_{3.3}\text{Co}_{0.2}\text{Si}_x$  ( $x = 0$  to  $0.2$ ) alloys: (a)  $\text{Si}_0$  alloy and (b)  $\text{Si}_{0.15}$  alloy.

boundaries could provide effective protection until the alloy is pulverized to a smaller grain size. Hence, it can be concluded that alloys with smaller grain sizes exhibit better cycle stabilities. The positive effect on cycle stability due to the addition of Si is attributed to the following two considerations. First, the addition of Si facilitates the formation of a dense silicon oxide layer on the alloy surface,<sup>[2,26]</sup> which effectively prevents alloy corrosion. Second, the enlarged cell volume caused by the addition of Si reduces the ratio of expansion/contraction in the process of hydrogen absorption/desorption, enhancing the anti-pulverization capability.

## 2. Activation capability and discharge capacity

The activation capability of an alloy electrode is evaluated by the number of charge–discharge cycles required to attain the maximum discharge capacity at a constant current density of 60 mA/g. A lower number of charging–discharge cycles corresponds to a better activation property. The cycle number dependencies of the discharge capacities of the as-cast and annealed  $\text{La}_{0.8}\text{Mg}_{0.2}\text{Ni}_{3.3}\text{Co}_{0.2}\text{Si}_x$  ( $x = 0$  to  $0.2$ ) are described in Figure 5. All the alloys attain their maximum discharge capacities at the first charge–discharge cycle, suggesting that the annealing treatment does not affect the activation capability of the alloy. The superior activation performances of the as-cast and annealed alloys result from their multiphase structures because the phase boundary not only decreases the lattice distortion and strain energy produced in the hydrogen absorption process, but also provides good diffusion tunnels for hydrogen atoms, which greatly improves the activation performance of the alloy. In addition, the enlarged cell volume produced by annealing reduces the expansion/contraction ratio of the alloy in the hydrogen absorption/desorption process, lowering the strain energy and diffusion activation energy.

The discharge capacities of the as-cast and annealed  $\text{La}_{0.8}\text{Mg}_{0.2}\text{Ni}_{3.3}\text{Co}_{0.2}\text{Si}_x$  ( $x = 0$  to  $0.2$ ) alloys as a function of annealing temperature are presented in Figure 6. Alloy discharge capacity first increases and then decreases with the increasing annealing temperature. When annealed at 1173 K (900 °C), the  $\text{Si}_0$ ,  $\text{Si}_{0.05}$ ,  $\text{Si}_{0.1}$ ,  $\text{Si}_{0.15}$ , and  $\text{Si}_{0.2}$  alloys yield maximum

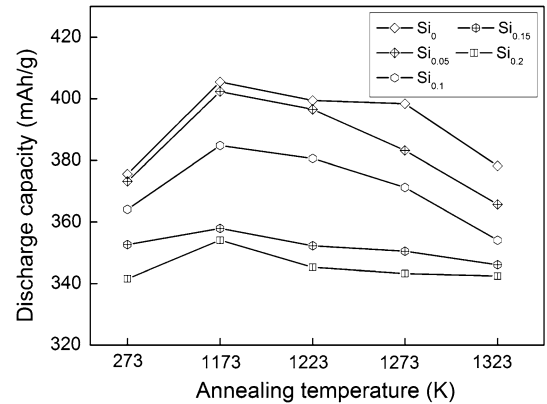


Fig. 6—Evolution of the discharge capacity of the  $\text{La}_{0.8}\text{Mg}_{0.2}\text{Ni}_{3.3}\text{Co}_{0.2}\text{Si}_x$  ( $x = 0$  to  $0.2$ ) alloys with annealing temperature.

discharge capacities of 405.5, 402.3, 384.8, 357.9, and 354.1 mAh/g, respectively. Figure 6 indicates that regardless of state, alloy discharge always decreases with the increasing Si content. The discharge capacity is reduced from 375.5 to 341.6 mAh/g for the as-cast alloy and from 405.5 to 354.1 mAh/g for the as-annealed [1173 K (900 °C)] alloy with the increasing Si content from 0 to 0.2.

The maximum discharge capacities of the alloys result from the change in alloy structure due to the annealing treatment. When the annealing temperature is 1173 K (900 °C), the abundance of the  $(\text{La},\text{Mg})_2\text{Ni}_7$  phase increases, and the cell volume enlarges; these effects both facilitate the improvement in discharge capacity. When the annealing temperature is above 1173 K (900 °C), the annealing decreases the abundance of the  $(\text{La},\text{Mg})_2\text{Ni}_7$  phase and increases that of the  $\text{LaNi}_5$  phase; this thus results in a decline in the discharge capacity since the  $(\text{La},\text{Mg})_2\text{Ni}_7$  phase possesses a much higher discharge capacity than the  $\text{LaNi}_5$  phase. The decrease in discharge capacity due to the addition of Si is ascribed to two aspects. First, the addition of Si plays a negative role on the discharge capacity of  $\text{LaNi}_5$  phase, which is universally acknowledged.<sup>[27,28]</sup> Second, the reduction in the abundance of  $(\text{La},\text{Mg})_2\text{Ni}_7$  resulting from the addition of Si is harmful to the discharge capacity of the alloy.

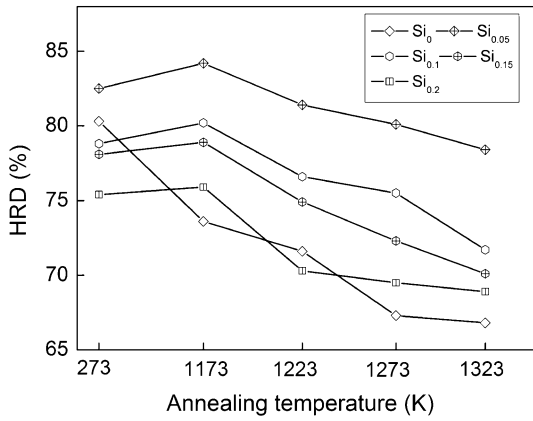
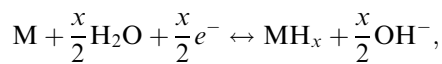


Fig. 7—Evolution of the HRD values of the  $\text{La}_{0.8}\text{Mg}_{0.2}\text{Ni}_{3.3}\text{Co}_{0.2}\text{Si}_x$  ( $x = 0$  to  $0.2$ ) alloys with annealing temperature.

### 3. Electrochemical hydrogen storage kinetics

The electrochemical hydrogen storage kinetics of an alloy electrode is evaluated by its high-rate discharge ability (HRD), which is defined as  $\text{HRD} = C_{900,\text{max}}/C_{60,\text{max}} \times 100$  pct, where  $C_{900,\text{max}}$  and  $C_{60,\text{max}}$  are the maximum discharge capacities of the alloy electrode charged and discharged at current densities of 900 and 60 mA/g, respectively. The evolutions of HRD values of the as-cast and annealed  $\text{La}_{0.8}\text{Mg}_{0.2}\text{Ni}_{3.3}\text{Co}_{0.2}\text{Si}_x$  ( $x = 0$  to  $0.2$ ) alloys with the discharge current density are demonstrated in Figure 7, from which it is found that the HRD value of the Si-free alloy always declines with the rising annealing temperature, while that of the Si-added alloys reaches maximum values under the same circumstances, namely 84.2, 80.2, 78.9, and 75.9 pct corresponding to the  $\text{Si}_{0.05}$ ,  $\text{Si}_{0.1}$ ,  $\text{Si}_{0.15}$ , and  $\text{Si}_{0.2}$  alloys, respectively. Although all the Si-added alloys annealed at 1173 K (900 °C) exhibit slightly increased HRD values, the general trend suggests that annealing actually negatively affects HRD.

A clear understanding of the mechanism of electrochemical hydriding/dehydriding is very necessary to better comprehend the influences of annealing on electrochemical hydrogen storage kinetics. The electrochemical hydriding/dehydriding reaction that takes place at the hydrogen storage electrode in an alkaline solution during the charging and discharging process can be summarized as follows:



where M is the hydrogen storage alloy. From the above equation, it can be seen that when the alloy electrode is charging in KOH solution, hydrogen atoms originating from electrolyzing  $\text{H}_2\text{O}$  diffuse from the interface between the alloy and electrolyte into the bulk alloy and then store themselves in the metallic lattice in the form of hydride. In the process of discharging, the hydrogen stored in the bulk alloy diffuses toward the surface, where it is oxidized. The hydrogen atoms adhering to the grain surface of the alloy electrode have two possible destinations: forming hydrogen molecules or diffusing into the bulk alloy, where they exist in the

form of hydride. This means that the diffusion rate of hydrogen atom on the surface layer of the alloy is simply the ratio of the diffusion current to the imposed current, which is a vital factor for determining the utilization of charging current. That is to say, the electrochemical hydrogen storage kinetics of the alloy electrode is determined by the charge-transfer rate on the surface of the alloy electrode along with the hydrogen diffusion capability in the bulk alloy.<sup>[29]</sup> Therefore, it seems to be absolutely inevitable to investigate the hydrogen diffusion coefficient and charge-transfer rate.

The charge-transfer ability on the surface of an alloy electrode can be qualitatively evaluated by its electrochemical impedance spectrum (EIS), as interpreted and modeled by Kuriyama *et al.*<sup>[30]</sup> The EIS curves of the as-cast and annealed  $\text{La}_{0.8}\text{Mg}_{0.2}\text{Ni}_{3.3}\text{Co}_{0.2}\text{Si}_x$  ( $x = 0$  to  $0.2$ ) alloys are displayed in Figure 8, from which it can be seen that each EIS spectrum contains two distorted capacitive loops at high and middle frequencies as well as an almost straight line at low frequency. The smaller semicircle in the high-frequency region symbolizes the contact resistance between the alloy powder and the conductive material, and the larger one in the middle-frequency region signifies the charge-transfer resistance on the alloy surface, while the line in low frequency emblemizes the atomic hydrogen diffusion in the alloy. Thereby, it seems to be self-evident that the larger the radius of the semicircle in the middle-frequency region is, the higher the charge-transfer resistance of the alloy electrode will be. Interestingly, the radii of the large semicircles of the  $\text{Si}_0$  alloy always swell with the rising annealing temperature, but those of the  $\text{Si}_{0.15}$  alloy first shrink and then expand in the same case, which is well consistent with the results provided in Figure 7.

Figure 9 exhibits the semilogarithmic curves of anodic current vs working duration of the as-cast and annealed  $\text{La}_{0.8}\text{Mg}_{0.2}\text{Ni}_{3.3}\text{Co}_{0.2}\text{Si}_x$  ( $x = 0$  to  $0.2$ ) alloys. The diffusion coefficient of the hydrogen atoms in the bulk of the alloy could be calculated through the slope of the linear region of the corresponding plots by the following formulae:<sup>[31]</sup>

$$\log i = \log \left( \pm \frac{6FD}{da^2} (C_0 - C_s) \right) - \frac{\pi^2 D}{2.303 a^2} t \quad [1]$$

$$D = - \frac{2.303 a^2 d \log i}{\pi^2 dt} \quad [2]$$

where  $i$  is the diffusion current density (A/g),  $D$  is the hydrogen diffusion coefficient ( $\text{cm}^2/\text{s}$ ),  $C_0$  is the initial hydrogen concentration in the bulk of the alloy ( $\text{mol}/\text{cm}^3$ ),  $C_s$  is the hydrogen concentration on the surface of the alloy particles ( $\text{mol}/\text{cm}^3$ ),  $a$  is the alloy particle radius (cm),  $d$  is the density of the hydrogen storage alloy ( $\text{g}/\text{cm}^3$ ), and  $t$  is the discharge time (s). In Eq. [2],  $\frac{d \log i}{dt}$  is the slope of the linear region shown in Figure 9. The annealing temperature dependence of the  $D$  values of the as-cast and annealed alloys are also inserted in Figure 9. Evidently, the  $D$  values of the  $\text{Si}_0$  alloy monotonically decline from  $5.95 \times 10^{-11}$  to  $5.08 \times 10^{-12} \text{ cm}^2/\text{s}$ , while the annealing temperature

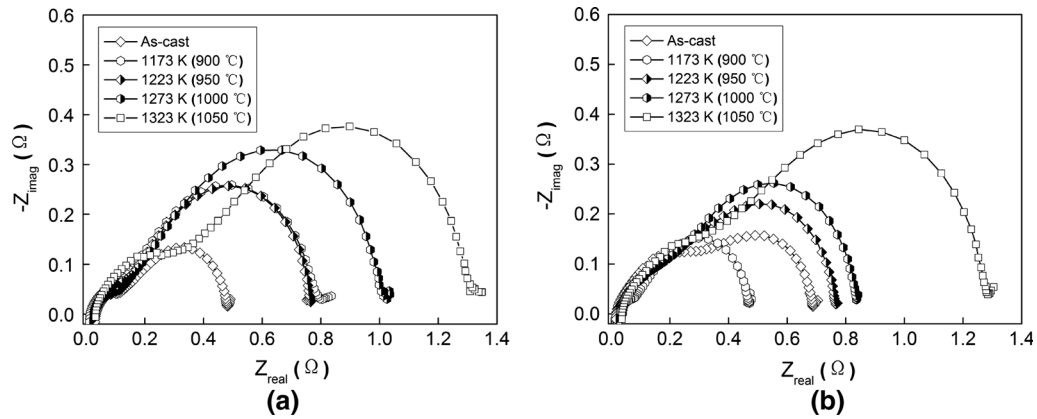


Fig. 8—Electrochemical impedance spectra (EIS) of the as-cast and annealed  $\text{La}_{0.8}\text{Mg}_{0.2}\text{Ni}_{3.3}\text{Co}_{0.2}\text{Si}_x$  ( $x = 0$  to  $0.2$ ) alloys: (a)  $\text{Si}_0$  alloy and (b)  $\text{Si}_{0.15}$  alloy.

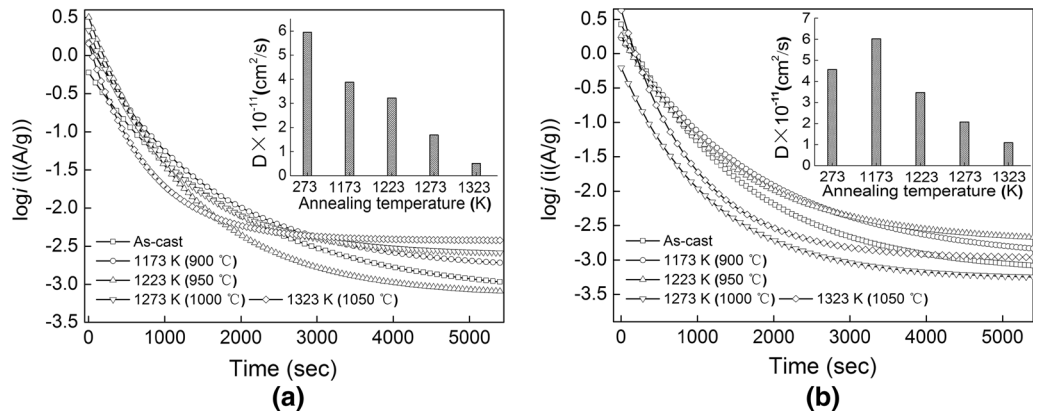


Fig. 9—Semi-logarithmic curves of anodic current vs time responses of the as-cast and annealed  $\text{La}_{0.8}\text{Mg}_{0.2}\text{Ni}_{3.3}\text{Co}_{0.2}\text{Si}_x$  ( $x = 0$  to  $0.2$ ) alloys: (a)  $\text{Si}_0$  alloy and (b)  $\text{Si}_{0.15}$  alloy.

grows from 0 [as-cast is defined as the annealing temperature of 273 K (0 °C)] to 1323 K (1050 °C), whereas that of the  $\text{Si}_{0.15}$  alloy reaches its maximum value of  $6.02 \times 10^{-11} \text{ cm}^2/\text{s}$  at the annealing temperature of 1173 K (900 °C), which is the same temperature at which the  $\text{Si}_{0.15}$  alloy exhibits its maximum HRD value as demonstrated in Figure 7.

Figure 10 displays the Tafel polarization curves of the as-cast and annealed  $\text{La}_{0.8}\text{Mg}_{0.2}\text{Ni}_{3.3}\text{Co}_{0.2}\text{Si}_x$  ( $x = 0$  to  $0.2$ ) alloys. We discover that, in all cases, there is a clear point of inflection in each anodic polarization curve, implying the presence of critical value which is termed as limiting current density ( $I_L$ ). It suggests that an oxidation reaction takes place on the surface of the alloy electrode, and the oxidation layer hinders hydrogen atoms from further penetrating.<sup>[32]</sup> Hence,  $I_L$  can be viewed as a critical current density of passivation that essentially depends on the diffusion rate of hydrogen in alloy electrode matrix.<sup>[29]</sup> The  $I_L$  values of the alloys as functions of annealing temperature are also provided in Figure 10, from which we note that the  $I_L$  values of the  $\text{Si}_0$  alloy drops from 2.13 to 1.138 A/g with the annealing temperatures rising from 0 K to 1323 K (−273 °C to 1050 °C), whereas that of the  $\text{Si}_{0.15}$  alloy exhibits a

maximum value of 2.26 A/g at an annealing temperature of 1173 K (900 °C).

In summary, the hydrogen diffusion coefficient ( $D$ ), electrochemical impedance spectra (EIS), and limiting current density ( $I_L$ ) decline with the increasing annealing temperature for Si-free alloys, whereas for Si-containing alloys, they reach maximum values as the annealing temperature increases. These variation tendencies are consistent with the relationship between HRD and annealing temperature for Si-free alloys and Si-added alloys, respectively. Based on the above-mentioned results, we can conclude that the HRD of the experimental alloys is jointly dominated by the charge-transfer rate and the hydrogen diffusion capability.

The diffusion coefficient of hydrogen atoms in metallic lattices is considered to depend on the strength of metal–hydrogen interactions as well as the structure of the alloy.<sup>[33]</sup> As considered by Cui *et al.*,<sup>[34]</sup> the increases of the lattice constants and cell volumes reduce the diffusion activation energy of hydrogen atoms, thus enhancing hydrogen diffusion. The diffusion ability of hydrogen atoms is also very sensitive to grain size<sup>[35]</sup> because grain boundaries can provide sites with lower activation energies for diffusion, facilitating the diffu-



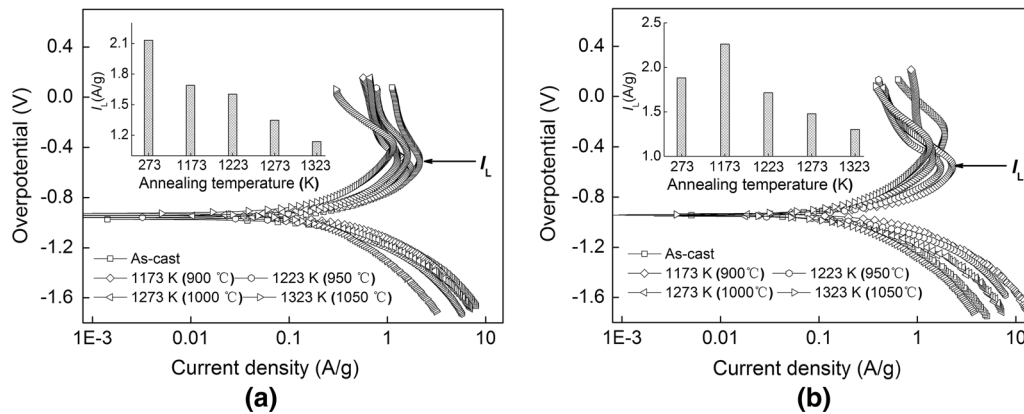


Fig. 10—Tafel polarization curves of the as-cast and annealed  $\text{La}_{0.8}\text{Mg}_{0.2}\text{Ni}_{3.3}\text{Co}_{0.2}\text{Si}_x$  ( $x = 0$  to  $0.2$ ) alloys: (a)  $\text{Si}_0$  alloy and (b)  $\text{Si}_{0.15}$  alloy.

sion of hydrogen atom in alloys. Based on the change in alloy structure generated by annealing, we can conclude that the annealing treatment has both positive and negative effects on the electrode hydrogen-storage kinetics. The positive contribution to the electrochemical kinetics is inarguably ascribed to the increased cell volumes induced by annealing, whereas the negative effects are attributed to the coarse grains that result from annealing. In fact, the electrochemical kinetics of the  $\text{Si}_0$  alloy always decrease with the increasing annealing temperature, suggesting that the effect of the grain boundaries on the electrochemical kinetics is predominant. The variations in the electrochemical kinetics of the Si-added alloys with the annealing temperature obviously reflect the positive and negative impacts, which can be ascribed to the addition of Si. The positive contribution of adding Si is affiliated with two aspects: on one hand, the enlarged cell volume due to Si addition reduces the diffusion activation energy of hydrogen atoms; on the other hand, the abundance of the  $\text{LaNi}_5$  phase increases when Si is added, which dramatically improves the electrocatalytic activity of the alloy electrodes. In contrast, the compact silicon oxide layer resulting from the addition of Si not only severely impairs the charge-transfer rate on the alloy surface but also hinders the hydrogen diffusion from the inner of the bulk to the surface, consequently weakening the electrochemical kinetic property.

#### IV. CONCLUSIONS

Annealing has been shown to have significant effects on the structures and electrochemical hydrogen-storage performances of  $\text{La}_{0.8}\text{Mg}_{0.2}\text{Ni}_{3.3}\text{Co}_{0.2}\text{Si}_x$  ( $x = 0$  to  $0.2$ ) electrode alloys. The major conclusions are summarized as follows:

1. Instead of altering the component phases, the annealing treatment results in notable changes in the abundances of the phases present in the alloy. The abundance of the  $(\text{La,Mg})_2\text{Ni}_7$  phase first increases and then declines with the increasing annealing temperature, whereas the  $\text{LaNi}_5$  phase exhibits the opposite trend. Meanwhile, the annealing treatment

clearly increases the lattice constants and cell volumes of the major phases and coarsens the grains of the alloys.

2. Although the annealing treatment does not affect the activation capability of the alloy, it significantly improves its cycle stability. Annealing at higher temperature [1323 K (1050 °C)] impairs the cycle stability of the alloy, which is primarily due to the grain coarsening caused by annealing. The discharge capacity of the alloy first increases and then decreases with the increasing annealing temperature.
3. The high-rate discharge abilities (HRDs) of the Si-added alloys reach maximum values when the annealing temperature is increased, whereas that of the Si-free alloy declines with the increasing annealing temperature. Similar trends are obtained for hydrogen diffusion coefficient ( $D$ ), limiting current density ( $I_L$ ), and electrochemical impedance spectra (EIS), suggesting that the HRD values of the experimental alloys depend on the charge-transfer rate along with the hydrogen diffusion capability.

#### ACKNOWLEDGMENTS

This work is financially supported by the National Natural Science Foundations of China (Nos. 51161015 and 51371094).

#### REFERENCES

1. B. Sakintuna, F. Lamari-Darkrim, and M. Hirscher: *Int. J. Hydrogen Energy*, 2007, vol. 32, pp. 1121–40.
2. J.J.G. Willems and K.H.J. Buschow: *J. Less-Common Met.*, 1987, vol. 129, pp. 13–30.
3. S.R. Ovshinsky, M.A. Fetcenko, and J. Ross: *Science*, 1993, vol. 260, pp. 176–81.
4. M. Tukahara, T. Kamiya, K. Takahashi, A. Kawabata, S. Sakurai, J. Shi, H.T. Takeshita, N. Kuriyama, and T. Sakai: *J. Electrochem. Soc.*, 2000, vol. 147, pp. 2941–44.
5. D. Sun, H. Enoki, F. Gingl, and E. Akiba: *J. Alloys Compd.*, 1999, vol. 285, pp. 279–83.
6. X.F. Li, L.Z. Wang, H.C. Dong, Y.H. Song, and H.D. Shang: *J. Alloys Compd.*, 2012, vol. 510, pp. 114–18.

7. B. Knosp, L. Vallet, and P. Blanchard: *J. Alloys Compd.*, 1999, vols. 293–295, pp. 770–74.
8. X.P. Song, P. Pei, P.L. Zhang, and G.L. Chen: *J. Alloys Compd.*, 2008, vol. 455, pp. 392–97.
9. J.H. Li, B.Z. Liu, S.M. Han, L. Hu, X. Zhao, and M.Z. Wang: *Rare Met.*, 2011, vol. 30, pp. 458–63.
10. Y.H. Zhang, C. Zhao, T. Yang, H.W. Shang, C. Xu, and D.L. Zhao: *J. Alloys Compd.*, 2013, vol. 555, pp. 131–37.
11. K. Kadir, T. Sakai, and I. Uehara: *J. Alloys Compd.*, 1997, vol. 257, pp. 115–21.
12. T. Kohno, H. Yoshida, F. Kawashima, T. Inaba, I. Sakai, M. Yamamoto, and M. Kanda: *J. Alloys Compd.*, 2000, vol. 311, pp. L5–7.
13. Y.F. Li, Y.H. Cao, L. Huang, M.X. Gao, and H.G. Pan: *J. Alloys Compd.*, 2011, vol. 509, pp. 675–86.
14. Y.F. Liu, H.G. Pan, M.X. Gao, and Q.D. Wang: *J. Mater. Chem.*, 2011, vol. 21, pp. 4743–55.
15. Y.F. Liu, H.G. Pan, M.X. Gao, R. Li, and Y.Q. Lei: *J. Alloys Compd.*, 2004, vol. 376, pp. 304–13.
16. Y.H. Zhang, B.W. Li, H.P. Ren, Y. Cai, X.P. Dong, and X.L. Wang: *J. Alloys Compd.*, 2008, vol. 458, pp. 340–45.
17. X.Q. Shen, Y.G. Chen, M.D. Tao, C.L. Wu, G. Deng, and Z.Z. Kang: *Int. J. Hydrogen Energy*, 2009, vol. 34, pp. 3395–3403.
18. Y.H. Zhang, T. Yang, Y. Cai, Z.H. Hou, H.P. Ren, and D.L. Zhao: *Rare Met.*, 2012, vol. 31, pp. 457–65.
19. X.Q. Shen, Y.G. Chen, M.D. Tao, C.L. Wu, G. Deng, and Z.Z. Kang: *Int. J. Hydrogen Energy*, 2009, vol. 34, pp. 2661–69.
20. Z.W. Dong, Y.M. Wu, L.Q. Ma, L.D. Wang, X.D. Shen, and L.M. Wang: *Int. J. Hydrogen Energy*, 2011, vol. 36, pp. 3050–55.
21. X.D. Wei, H. Dong, Y.G. Liu, P. Zhang, J.W. Zhu, and G. Yu: *J. Alloys Compd.*, 2009, vol. 481, pp. 687–91.
22. T.Z. Huang, X.X. Yuan, J.M. Yu, Z. Wu, J.T. Han, G.X. Sun, N.X. Xu, and Y.H. Zhang: *Int. J. Hydrogen Energy*, 2012, vol. 37, pp. 1074–79.
23. Y.H. Zhang, B.W. Li, H.P. Ren, Y. Cai, X.P. Dong, and X.L. Wang: *Int. J. Hydrogen Energy*, 2007, vol. 32, pp. 4627–34.
24. M. Dornheim, S. Doppiu, G. Barkhordarian, U. Boesenberg, T. Klassen, O. Gutfleisch, and R. Bormann: *Scripta Mater.*, 2007, vol. 56, pp. 841–46.
25. T. Sakai, T. Hazama, H. Miyamura, N. Kuriyama, A. Kato, and H. Ishikawa: *J. Less-Common Met.*, 1991, vols. 172–174, pp. 1175–84.
26. J.J.G. Willems: *Philips J. Res.*, 1984, vol. 39, pp. 1–94.
27. T. Sakai, K. Oguro, H. Miyamura, N. Kuriyama, A. Kato, H. Ishikawa, and C. Iwakura: *J. Less-Common Met.*, 1990, vol. 161, pp. 193–202.
28. F. Meli, A. Zuetzel, and L. Schlapbach: *J. Alloys Compd.*, 1992, vol. 190, pp. 17–24.
29. B.V. Ratnakumar, C. Witham, Jr, R.C. Bowman, A. Hightower, and B. Fultz: *J. Electrochem. Soc.*, 1996, vol. 143, pp. 2578–84.
30. N. Kuriyama, T. Sakai, H. Miyamura, I. Uehara, H. Ishikawa, and T. Iwasaki: *J. Alloys Compd.*, 1993, vol. 202, pp. 183–97.
31. G. Zheng, B.N. Popov, and R.E. White: *J. Electrochem. Soc.*, 1995, vol. 142, pp. 2695–98.
32. X.Y. Zhao, Y. Ding, L.Q. Ma, L.Y. Wang, M. Yang, and X.D. Shen: *Int. J. Hydrogen Energy*, 2008, vol. 33, pp. 6727–33.
33. F. Feng and D.O. Northwood: *J. Power Sources*, 2004, vol. 136, pp. 346–50.
34. N. Cui and J.L. Luo: *Int. J. Hydrogen Energy*, 1999, vol. 24, pp. 37–42.
35. D.H. Xie, P. Li, C.X. Zeng, J.W. Sun, and X.H. Qu: *J. Alloys Compd.*, 2009, vol. 478, pp. 96–102.